European Journal of Mechanics / A Solids 117 (2026) 106008

Contents lists available at ScienceDirect

European Journal of Mechanics / A Solids

journal homepage: www.elsevier.com/locate/ejmsol

Full length article

Finite element analysis of non-uniform functionally graded multi-cracked Timoshenko beams using an equilibrium-based formulation

H.A.F.A. Santos [a,*], V.V. Silberschmidt [b]

[a] Departamento de Engenharia Mecânica, UnIRE, Instituto Superior de Engenharia de Lisboa, Rua Conselheiro Emídio Navarro, 1, Lisboa, 1959-007, Portugal
[b] Wolfson School of Mechanical, Electrical and Manufacturing Engineering, Loughborough University, Wolfson Building, Ashby Rd, Loughborough, LE11 3TU, UK

ARTICLE INFO

Keywords:
FGM beams
Non-uniform cross-sections
Timoshenko theory
Cracks
Finite element method
Equilibrium-based formulation

ABSTRACT

A novel finite element formulation is introduced for the static analysis of non-uniform functionally graded multi-cracked Timoshenko beams with small deformations. The cracks, assumed to remain open, are modelled using the so-called discrete spring approach, in which Dirac delta generalized functions are introduced into the bending flexibility of the beams. The formulation is derived on the basis of a complementary variational approach that involves only the elements' shear forces and bending moments as the fundamental unknown fields. The corresponding element flexibility matrix is obtained in closed-form, with the crack contributions explicitly separated from the standard bending and shear flexibility terms. The numerical solutions produced by the formulation are strictly equilibrated, *i.e.*, they satisfy all equilibrium conditions of the associated boundary-value problem in strong form. The effectiveness and accuracy of the formulation are numerically assessed through its application to several benchmark problems. The obtained results are analysed and compared, where possible, to exact (or reference) solutions and solutions given by the standard displacement-based finite element formulation, clearly illustrating the capability of the formulation to deliver highly accurate results for both thin and thick beams, even on meshes with only a few degrees-of-freedom.

1. Introduction

The presence of damage significantly influences the performance of structures, potentially resulting in various types and degrees of failure, from reduced serviceability to a total loss of functionality. Consequently, the effects of structural damage have been thoroughly explored across multiple disciplines, including Civil, Mechanical, and Aeronautical Engineering, particularly with the goal of developing more accurate and efficient models.

One-dimensional beam models are regarded as fundamental tools in structural analysis. In particular, they have been widely used to study the mechanical response of cracked beams (Petroski, 1981), as they require low computational effort while effectively capturing the global behaviour of cracked elements. The classical Euler–Bernoulli and Timoshenko beam theories have been further developed to account for local variations in material properties and geometric parameters. Methodologies for modelling cracked beams can be classified into three main categories (Dimarogonas, 1996): (i) local stiffness reduction models (Pandey and Biswas, 1994); (ii) continuous models (Christides and Barr, 1984); and (iii) discrete spring (or lumped flexibility) models (Bilello, 2001). Among these, the discrete spring approach has been recognized as the most widely used method for assessing the global response of cracked beams. Within this approach: (i) cracks are represented as internal rotational springs, whose stiffness depends on the crack size and cross-sectional geometry; (ii) crack initiation and propagation are neglected (Friswell and Penny, 2002); and (iii) cracks are generally assumed to remain open throughout the loading process (linear open-crack model). While several definitions of the stiffness of rotational springs can be found in the literature, the first definition for a rectangular cross-section appears to be due to Okamura et al. (1969). Each spring connects two adjacent uncracked segments of the beam, which are modelled as elastic elements. The domains of these segments are characterized by continuous response functions, while enforcing the necessary continuity and discontinuity conditions between adjacent segments. Specifically, this approach enforces the continuity of displacements, bending moments, and shear forces, and introduces a discontinuity in the rotation of the cracked cross-section proportional to the transmitted bending moment. However, the computational effort required by this procedure increases with the number of cracks, and, more importantly, it does not allow closed-form (explicit) expressions for the solution to be obtained. An alternative strategy is based on modelling crack discontinuities through the so-called *generalized Dirac delta function*, as proposed by Biondi and Caddemi (2005, 2007). In

* Corresponding author.
E-mail address: hugo.santos@isel.pt (H.A.F.A. Santos).

https://doi.org/10.1016/j.euromechsol.2025.106008
Received 23 September 2025; Received in revised form 9 November 2025; Accepted 24 December 2025
Available online 24 December 2025

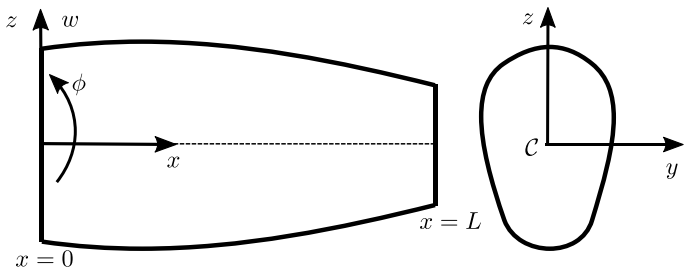

Fig. 1. Undamaged beam geometry and configuration.

this approach, the singularities induced by the cracks are introduced as negative impulses in the flexural stiffness by means of Dirac delta functions with a negative sign — *rigidity modelling*. However, such representation is not consistent with the positive-definite nature of flexural stiffness. To overcome this inconsistency, Palmeri and Cicirello (2011) proposed an alternative representation of cracks, in which Dirac delta functions with a positive sign are introduced into the bending flexibility of the cracked beam – *flexibility modelling approach*. This latter approach was later theoretically justified by Caddemi and Morassi (2013).

In Cicirello and Palmeri (2014), the linear open-crack model was extended to beams with switching cracks, *i.e.*, cracks whose state alternates between open and closed depending on the sign of the axial strain at their centre and on their position along the beam (either on the top or the bottom surface). A different strategy was proposed by Yang et al. (2016), in which the effect of the crack gap on the bending deformation of the beam was taken into account within the framework of the switching-crack model. Donà et al. (2015) proposed a new multi-damaged beam element with shear deformation, in which a crack was modelled as a set of longitudinal, rotational, and transverse elastic springs.

Although beam elements with variable cross-sections – either continuous or stepwise – are commonly employed in engineering design to reduce weight, optimize strength and stability, or satisfy specific architectural and functional requirements, most studies available in the literature focus on the analysis of uniform cracked beams, *i.e.*, beams with constant cross-sections. Exceptions include the works of Failla and Impollonia (2012), Skrinar (2013), Skrinar and Imamovic (2018) and Skrinar (2019), in which thin beams with cross-sections varying along the axial coordinate (*i.e.*, non-uniform beams) were considered.

Due to their outstanding structural performance, functionally graded materials (FGMs) have been increasingly employed in recent years across a wide range of engineering applications, including submarines, automotive components, space structures, and biomedical devices. FGMs are inhomogeneous composites whose properties vary continuously with respect to spatial coordinates. Their material composition can be tailored to enhance strength, toughness, and high-temperature resistance, among other properties, in order to meet specific structural performance requirements.

Several studies on the numerical modelling of cracked FGM beams – particularly those addressing free vibration and/or buckling analyses (Yang and Chen, 2008; Kitipornchai et al., 2009; Alshorbagy et al., 2011; Wei et al., 2012; Lien et al., 2017; Rajasekaran and Khaniki, 2018; Shabani and Cunedioglu, 2020b; Sinha and Kumar, 2021) and crack identification (Zhu et al., 2019; Hassaine et al., 2025) – can be found in the literature. However, research works concerning non-uniform cracked FGM beams remain very limited. Notable exceptions include the study by Shabani and Cunedioglu (2020a), which focused on the free vibration analysis of cantilever Timoshenko beams of rectangular cross-section with constant height but variable (exponential or linear) width, and, more recently, the work by Nguyen et al. (2024), which addressed the free vibration analysis of non-uniform cracked axially graded beams.

Although most of the previously discussed studies primarily focus on deriving analytical (closed-form) solutions, the presence of multi-span configurations, advanced constitutive laws, and/or complex beam geometries or loading conditions can make the derivation of such solutions highly challenging or even impossible. Several numerical methods have been proposed in the literature for modelling complex structural problems. Among these, the finite element method (FEM) has emerged as the most widely used technique (Zienkiewicz et al., 2005; Zienkiewicz and Taylor, 2005). Among the different FEM formulations, the displacement-based approach remains the most common and widely adopted. However, when applied to Timoshenko beam models, the standard low-order displacement-based finite element formulation – employing C^0-continuous, piecewise-linear approximations for both transverse displacements and rotations – suffers from the so-called *shear-locking phenomenon* in the thin-beam limit, leading to erroneous results (Baier-Saip et al., 2020). Although several techniques exist to alleviate or eliminate shear-locking, such as reduced integration, assumed strains, or mixed interpolation techniques (Hughes, 2012), conventional displacement-based formulations applied to Timoshenko beams still yield discontinuous distributions of bending moments and internal forces. Formulations that can produce strictly equilibrated solutions and that are naturally free from shear-locking are the so-called *equilibrium-based formulations*. Examples of such formulations, applied to homogeneous and uniform beams – in either geometrically linear or geometrically nonlinear settings – were proposed in, *e.g.*, Santos et al. (2011), Santos (2011, 2012), Santos and Silberschmidt (2014), Santos (2015, 2020) and Santos (2024).

In our recent conference paper (Santos and Silberschmidt, 2024), we introduced an equilibrium-based formulation for the static analysis of non-uniform functionally graded multi-cracked Timoshenko beams and presented preliminary numerical results. The present work extends that study by further developing the formulation and demonstrating its full capabilities for the numerical analysis of single- or multi-cracked, homogeneous or functionally graded, and uniform or non-uniform beams under various boundary conditions. The formulation is developed based on (i) a hybrid complementary variational approach, which relies on the discretization of the elements' shear forces and bending moments (statical variables), and (ii) the discrete spring model of cracks, in which Dirac delta generalized functions are introduced into the bending flexibility of the beams. Although the formulation employs the statical quantities as its fundamental unknowns – unlike the classical displacement-based formulation, which uses the kinematic quantities as its primary unknowns – a new, simple yet effective numerical algorithm has been devised to compute the kinematic quantities while properly accounting for the singularities induced by the cracks.

2. Boundary-value problem

2.1. Non-uniform FGM undamaged Timoshenko beam

Consider a planar, initially straight, non-uniform FGM undamaged beam with a symmetric cross-section about the z-axis, as illustrated in Fig. 1. The beam geometry is described by its centroidal axis, denoted

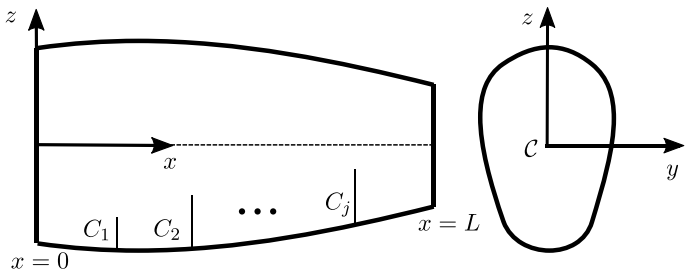

Fig. 2. Multi-cracked beam geometry and configuration.

by $\mathcal{C}$, parameterized by $x \in [0, L]$, where L is the total length of the beam. The domain $\mathcal{C}$ is decomposed into an internal part $\Omega =]0, L[$ and a boundary part $\Gamma = \Gamma_N \cup \Gamma_D = \{0, L\}$, where Γ_N and Γ_D denote the Neumann and Dirichlet boundaries, respectively, with $\Gamma_N \cap \Gamma_D = \emptyset$. The beam cross-section has a width b and a height h, both of which generally vary along the axial coordinate x.

Let the beam be subjected to a distributed transverse load $q(x)$ and a distributed bending moment $m(x)$, both applied along Ω. In addition, a concentrated force $\bar{V}$ and a concentrated moment $\bar{M}$ act on Γ_N, while a prescribed displacement $\bar{w}$ and a prescribed rotation $\bar{\phi}$ are defined on Γ_D. The quantities q, $\bar{V}$ and $\bar{w}$ are transverse (translational) quantities, whereas m, $\bar{M}$ and $\bar{\phi}$ are rotational ones. All loads are assumed to act along the centroidal axis of the beam.

The kinematic differential equations are given as

$$\gamma = \phi - w', \quad \chi = \phi', \text{ in } \Omega \tag{1}$$

where γ is the shear deformation, taken into account by means of the well-known Timoshenko beam theory, and χ is the bending curvature of the beam; $(\cdot)'$ denotes the derivative of $(\cdot)$ with respect to x.

The Dirichlet (or kinematic) boundary conditions are given as follows

$$w - \bar{w} = 0, \quad \phi - \bar{\phi} = 0, \text{ on } \Gamma_D \tag{2}$$

where w is the transverse displacement field of the beam axis and ϕ is the cross-section rotation of the beam, as represented in Fig. 1.

The equilibrium differential equations are given by

$$V' + q(x) = 0, \quad -M' + V + m(x) = 0, \text{ in } \Omega \tag{3}$$

which represent equilibrium of shear forces and bending moments, respectively.

The Neumann (or static) boundary conditions of the problem are

$$nV + \bar{V} = 0, \quad nM - \bar{M} = 0, \text{ on } \Gamma_N \tag{4}$$

with

$$n = \begin{cases} 1 & \text{if } x = L \\ -1 & \text{if } x = 0 \end{cases}$$

With regard to the material behaviour of a FGM beam, the following three categories are found in the literature: only axially graded behaviour (denoted here as A-FGM); only transversely graded behaviour (T-FGM); or both axially and transversely graded behaviour (A-T-FGM). The first two cases are the most adopted ones. The present study focuses on A-FGM beams. The constitutive relationships of a linear elastic A-FGM beam are as follows

$$V = C_s \gamma, \quad M = C_b \chi, \text{ in } \Omega \tag{5}$$

where C_s and C_b represent the shear and bending stiffnesses of the beam, respectively, given by

$$C_s(x) = \int_A f_s G(x)\, dA, \quad C_b(x) = \int_A E(x) z^2\, dA \tag{6}$$

in which E and G are the Young's and shear moduli, respectively, such that

$$G(x) = \frac{E(x)}{2(1+\nu)} \tag{7}$$

with ν the Poisson's ratio of the material, which, without loss of generality, is assumed as constant. f_s is the standard shear correction factor.

Although the proposed formulation can also handle T-FGM and A-T-FGM responses, it is believed that, due to their peculiar characteristics when combined with damage, such cases warrant a separate and dedicated study.

Substituting the kinematic differential Eqs. (1) into the constitutive relationships (5) yields

$$V = C_s(\phi - w'), \quad M = C_b \phi', \text{ in } \Omega \tag{8}$$

2.2. Non-uniform FGM multi-cracked Timoshenko beam

Consider now a FGM beam with multiple open edge cracks, aligned with the z-axis, as shown in Fig. 2. The cracks are denoted by C_j, with $j = 1, 2, \ldots, n_c$, where n_c stands for the total number of cracks in the beam.

A cracked beam is herein modelled using the so-called *discrete spring model*. In this approach, the beam is represented as an assembly of undamaged segments, while the cracks are modelled by equivalent springs. For slender beams in bending, the presence of cracks primarily affects the bending stiffness. A common way to account for this effect is to introduce an elastic hinge with rotational stiffness at the crack location. The stiffness of the equivalent spring is determined based on the severity of the associated damage, following the principles of linear fracture mechanics. Several expressions have been proposed in the literature for evaluating the equivalent rotational spring stiffness; see, *e.g.*, Okamura et al. (1969), Ostachowicz and Krawczuk (1991), Dimarogonas (1996), Chondros et al. (1998) and Bilello (2001). In most of these works, the stiffness is expressed in terms of the crack depth.

Following the flexibility modelling approach proposed by Palmeri and Cicirello (2011), a generic crack j, located at $x = \bar{x}_j$, with $0 < \bar{x}_j < L$, is modelled herein using the discrete spring approach, in which Dirac delta generalized functions are introduced into the bending flexibility of the beam as

$$\frac{1}{C_b^r} = \frac{1 + \sum_{j=1}^{n_c} \beta_j \delta(x - \bar{x}_j)}{C_b} \tag{9}$$

δ is the Dirac delta function as defined in the Appendix, and β_j is the coefficient related to the crack severity, given as

$$\beta_j = \frac{C_b(\bar{x}_j)}{K_j} \tag{10}$$

Herein, K_j is the rotational spring stiffness associated with crack j. Note that, C_b represents the undamaged bending stiffness of the beam, whereas C_b^r is the reduced (damaged) bending stiffness of the corresponding cracked beam.

Considering, for instance, a crack of uniform depth d_j, located in a rectangular cross-section with width b and height h, the equivalent rotational spring stiffness is given by Caddemi and Calio (2009) and Dimarogonas et al. (2013)

$$K_j = \frac{C_b(\bar{x}_j)}{h_j f(\xi_j)} \tag{11}$$

with $h_j = h(\bar{x}_j)$. $\xi_j = d_j/h_j$ is the dimensionless crack depth and $f(\xi_j)$ is the dimensionless local flexibility.

Although several definitions of local flexibility can be found in the literature, the earliest one appears to be that proposed by Okamura et al. (1969), in which $f(\xi_j)$ takes the form

$$f(\xi_j) = 6(1-\nu^2)(1.98\xi^2 - 3.277\xi^3 + 14.43\xi^4 - 31.26\xi^5 + 63.56\xi^6 - 103.36\xi^7 + 147.52\xi^8 - 127.69\xi^9 + 61.50\xi^{10}) \tag{12}$$

Notably, this approach depends on Poisson's ratio, with $\nu = 0$ for plane stress conditions and $\nu \neq 0$ for plane strain conditions. A slightly different but closely related formula was proposed by Rizos et al. in Rizos et al. (1990) as follows

$$f(\xi_j) = 5.346(1.8624\xi_j^2 - 3.95\xi_j^3 + 16.375\xi_j^4 - 37.226\xi_j^5 + 76.81\xi_j^6 - 126.9\xi_j^7 + 172\xi_j^8 - 143.97\xi_j^9 + 66.56\xi_j^{10}) \tag{13}$$

Alternatively, one of the simplest approaches is that proposed by Bilello (2001), which is valid only for beams with uniform rectangular cross-sections. According to this approach, the dimensionless local flexibility is expressed as

$$f(\xi_j) = \frac{\xi_j(2-\xi_j)}{0.9(\xi_j-1)^2} \tag{14}$$

Other formulations for the equivalent rotational stiffness of beams with rectangular cross-sections can be found in the literature. However, most of these yield very similar results, particularly for low levels of crack severity (*i.e.*, small crack depths). Formulations for beams with different cross-section geometries are also available in the literature; see, *e.g.*, Papadopoulos (2004) and the references therein. All three definitions of local flexibility presented above, (12), (13), and (14), were tested and compared in the numerical examples discussed in Section 5.

It should be noted that the influence of cracks on shear deformation is neglected in this study.

3. Variational basis: Complementary-energy-based principle

Variational principles play a fundamental role in solid and structural mechanics (Washizu, 1975), providing both a systematic means for deriving governing equations and boundary conditions and a rigorous foundation for developing consistent approximate formulations, as exemplified by the principles of stationary potential energy and stationary complementary energy, which yield kinematically and statically admissible weak-form solutions, respectively.

This study develops a complementary energy-based formulation for non-uniform FGM multi-cracked Timoshenko beams.

Following the methodology presented by Santos (2012), Santos and Silberschmidt (2014) and Santos (2015), the total complementary energy of a non-uniform FGM multi-cracked Timoshenko beam, $\Pi_c : \mathcal{U}_s(\Omega) \to \mathcal{R}$, can be expressed as follows

$$\Pi_c(M,V) = -U_c(M,V) + \Pi_{c,ext}(M,V) \tag{15}$$

where U_c is the complementary strain energy given by

$$U_c = \frac{1}{2}\int_0^L \left(\frac{M^2}{C_b^r} + \frac{V^2}{C_s}\right) dx \tag{16}$$

and $\Pi_{c,ext}$ is the external complementary energy given by

$$\Pi_{c,ext}(M,V) = [nM\bar{\phi}]_{\Gamma_D} + [nV\bar{w}]_{\Gamma_D} \tag{17}$$

U_c can be rewritten by separating the complementary strain energy of the undamaged beam from that associated with the cracks as follows

$$U_c = \frac{1}{2}\int_0^L \left(\frac{M^2}{C_b} + \frac{V^2}{C_s}\right) dx + \frac{1}{2}\sum_{j=1}^{n_c}\frac{M_j^2}{K_j} \tag{18}$$

with $M_j = M(\bar{x}_j)$. The last term in (18) represents the contribution of the n_c cracks to the complementary strain energy of the cracked beam and can be interpreted as the sum of the complementary strain energies of the rotational springs formally equivalent to the cracks.

$\mathcal{U}_s$ denotes the statically admissible space defined as

$$\mathcal{U}_s = \{(M,V) \in \mathcal{H}^1(\Omega)\times\mathcal{H}^1(\Omega) | \; -M' + V + m(x) = 0,\; V' + q(x) = 0 \text{ in } \Omega; \; nM - \bar{M} = 0,\; nV + \bar{V} = 0 \text{ on } \Gamma_N\}$$

where $\mathcal{H}^1$ is the standard first-order Sobolev space of square-integrable functions with square-integrable first derivatives.

It can also be shown that (M,V) is a stationary point of Π_c if, and only if, the following condition holds

$$\delta\Pi_c = 0,\; \forall\, (\delta M, \delta V) \in \mathcal{V}_s \tag{19}$$

where $\mathcal{V}_s$ is the homogeneous statically admissible space defined as

$$\mathcal{V}_s = \{(\delta M, \delta V) \in \mathcal{H}^1(\Omega)\times\mathcal{H}^1(\Omega) | \; -\delta M' + \delta V = 0,\; \delta V' = 0 \text{ in } \Omega; \; n\delta M = 0,\; n\delta V = 0,\; \text{on } \Gamma_N\}$$

Statement (19) expresses the principle of stationary complementary energy associated with the boundary-value problem under consideration. The finite element formulation presented below is developed on the basis of this variational principle.

4. Equilibrium-based finite element formulation

4.1. Finite element approximations

A finite element approximation of Eq. (19) consists of seeking $(M^h, V^h) \in \mathcal{U}_s^h$ such that Eq. (19) is satisfied for all $(\delta M^h, \delta V^h) \in \mathcal{V}_s^h$, where $\mathcal{U}_s^h \subset \mathcal{U}_s$ and $\mathcal{V}_s^h \subset \mathcal{V}_s$ are the discretized statically admissible spaces.

Assume that the entire domain Ω is partitioned into subdomains $\Omega_e \subset \Omega$, such that $\Omega = \bigcup_{e=1}^{n_e}\Omega_e$, where n_e denotes the number of beam elements. If the inter-element equilibrium conditions and the Neumann boundary conditions are relaxed within the framework of the complementary energy principle, the following augmented Lagrangian (or hybrid complementary energy) formulation must be considered

$$L_c = \sum_{e=1}^{n_e}\Pi_{c,e} + \sum_{i=1}^{n_{int}}\left(\lambda_i^V [\![V]\!]_{\Gamma_i} + \lambda_i^M [\![M]\!]_{\Gamma_i}\right) \tag{20}$$

where n_{int} denotes the number of inter-element boundaries, and Γ_i represents the ith inter-element boundary. $[\![(\cdot)]\!]$ denotes the jump of $(\cdot)$ across Γ_i. The Lagrange multipliers λ_i^V and λ_i^M, defined on Γ_i, are energy-conjugate to V and M, respectively, corresponding to the transverse displacements and rotations at the ends of the beam elements.

The finite element functions assumed for the shear force and bending moment fields are defined as

$$V^h(x) = s_1 - \int q(x)\, dx \tag{21a}$$

$$M^h(x) = s_2 + \int V^h(x)\, dx + \int m(x)\, dx = s_2 + s_1 x + M_p(x) \tag{21b}$$

where s_1 and s_2 are the shear force and bending moment element parameters, respectively. M_p denotes a particular solution of the equilibrium differential Eqs. (3), and is given by

$$M_p(x) = \int m(x)\, dx - \int^2 q(x)\, dx^2 \tag{22}$$

where $\int^2(\cdot)\, dx^2$ denotes the second-order primitive of $(\cdot)$. These fields satisfy the strong form of the equilibrium Eqs. (3), *i.e.*, they are such that $(M^h, V^h) \in \mathcal{U}_s^h$. Therefore, as long as M_p is exact and the integrations that appear in the complementary strain energy given by Eq. (16) are performed exactly, the resulting solutions for the shear force and bending moment fields are also exact.

4.2. Governing system of equations

The stationarity of the discrete form of the augmented Lagrangian (20), which is expressed as

$$\delta L_c^h = 0 \tag{23}$$

yields the following governing system of linear equations

$$\begin{bmatrix} \boldsymbol{F} & \boldsymbol{A}^T \\ \boldsymbol{A} & \boldsymbol{O} \end{bmatrix} \begin{bmatrix} \boldsymbol{s} \\ \boldsymbol{\lambda} \end{bmatrix} = \begin{bmatrix} \boldsymbol{d} \\ \boldsymbol{f} \end{bmatrix} \tag{24}$$

The system involves the element parameters and the Lagrange multipliers as unknowns. Here, $\boldsymbol{s}$ denotes the global vector of element parameters (collecting all s_i constants), and $\boldsymbol{\lambda}$ is the global vector of Lagrange multipliers, collecting the transverse displacements and rotations at the ends of the beam elements. $\boldsymbol{F}$ and $\boldsymbol{A}$ are the global flexibility and equilibrium matrices, respectively; $\boldsymbol{d}$ is the global vector of displacements and rotations due to the applied distributed loads, and $\boldsymbol{f}$ is the global vector of applied forces and moments. The structures of $\boldsymbol{F}$ and $\boldsymbol{d}$, defined at the element level, are provided in Section 4.3. Matrix $\boldsymbol{A}$ and vector $\boldsymbol{f}$ are defined only at the global level, and depend on the chosen discretization and the static boundary conditions of the problem.

4.3. Finite element matrices

Consider the vector that collects the element (shear force and bending moment) degrees-of-freedom defined as

$$\boldsymbol{s}_e = \begin{bmatrix} s_1 \\ s_2 \end{bmatrix} \tag{25}$$

With this ordering of the element degrees-of-freedom, and using the element approximation functions for the shear force and bending moment given in Eq. (21), the element flexibility matrix can be expressed as follows

$$\boldsymbol{F}_e = \boldsymbol{F}_e^b + \boldsymbol{F}_e^s + \boldsymbol{F}_e^c \tag{26}$$

with $\boldsymbol{F}_e^b$, $\boldsymbol{F}_e^s$ and $\boldsymbol{F}_e^c$ given by

$$\boldsymbol{F}_e^b = \begin{bmatrix} \int_0^{L_e} \frac{x^2}{C_b(x)}\,dx & \int_0^{L_e} \frac{x}{C_b(x)}\,dx \\ \int_0^{L_e} \frac{x}{C_b(x)}\,dx & \int_0^{L_e} \frac{1}{C_b(x)}\,dx \end{bmatrix}, \quad \boldsymbol{F}_e^s = \begin{bmatrix} \int_0^{L_e} \frac{1}{C_s(x)}\,dx & 0 \\ 0 & 0 \end{bmatrix},$$

$$\boldsymbol{F}_e^c = \sum_{j=1}^{n_c} \frac{1}{K_j} \begin{bmatrix} \bar{x}_j^2 & \bar{x}_j \\ \bar{x}_j & 1 \end{bmatrix} \tag{27}$$

where $0 < \bar{x}_j < L_e$, with L_e the length of the beam element Ω_e. $\boldsymbol{F}_e^b$ and $\boldsymbol{F}_e^s$ denote the contributions of bending and shear deformations, respectively, to the flexibility matrix of the undamaged beam element, while $\boldsymbol{F}_e^c$ represents the additional flexibility due to the cracks. Notably, this explicit separation avoids the numerical difficulties that often arise when the singular terms associated with the cracks must be evaluated using numerical integration, see, *e.g.*, Eftekhari (2015).

The element vector of displacements and rotations resulting from the applied distributed loads is given by

$$\boldsymbol{d}_e = \boldsymbol{d}_e^b + \boldsymbol{d}_e^s + \boldsymbol{d}_e^c \tag{28}$$

with

$$\boldsymbol{d}_e^b = \begin{bmatrix} \int_0^{L_e} \frac{x M_p(x)}{C_b(x)}\,dx \\ \int_0^{L_e} \frac{M_p(x)}{C_b(x)}\,dx \end{bmatrix}, \quad \boldsymbol{d}_e^s = \begin{bmatrix} \int_0^{L_e} \frac{\int^2 q(x)\,dx^2}{C_s(x)}\,dx \\ 0 \end{bmatrix}, \quad \boldsymbol{d}_e^c = \begin{bmatrix} \frac{\bar{x}_j M_p(\bar{x}_j)}{K_j} \\ \frac{M_p(\bar{x}_j)}{K_j} \end{bmatrix} \tag{29}$$

Here, $\boldsymbol{d}_e^b$, $\boldsymbol{d}_e^s$ and $\boldsymbol{d}_e^c$ denote the contributions of bending deformation, shear deformation, and cracks, respectively, to the generalized displacement vector of a beam element.

For complex cross-section variations and/or material behaviours, the integrations required to compute the element flexibility matrices and generalized displacement vectors may not be analytically feasible, necessitating the use of numerical quadrature. Nevertheless, irrespective of the integration method employed, the numerical solutions produced by the formulation remain statically admissible. Furthermore, as demonstrated in Section 5, highly accurate solutions can be obtained even with meshes consisting of only a few elements.

4.4. Computation of the kinematic fields

The kinematic fields ϕ and w at the element level are obtained by integrating Eqs. (8) along the elements, which yields

$$\phi(x) = \phi_p(x) + \phi_h(x) \tag{30a}$$

$$w(x) = w_p(x) + w_h(x) \tag{30b}$$

where (ϕ_p, w_p) are the particular solutions given by

$$\phi_p(x) = \int \frac{M_p(x)}{C_b(x)}\,dx + \sum_{j=1}^{n_c} \frac{M_p(\bar{x}_j)}{K_j} H(x - \bar{x}_j) \tag{31a}$$

$$w_p(x) = \int^2 \frac{M_p(x)}{C_b(x)}\,dx^2 - \int \gamma_p(x)\,dx + \sum_{j=1}^{n_c} \frac{M_p(\bar{x}_j)}{K_j}(x - \bar{x}_j) H(x - \bar{x}_j) \tag{31b}$$

and (ϕ_h, w_h) are the homogeneous solutions given by

$$\phi_h(x) = \int \frac{s_2 + s_1 x}{C_b(x)}\,dx + \frac{s_2 + s_1 \bar{x}_j}{K_j} H(x - \bar{x}_j) + c_\phi \tag{32a}$$

$$w_h(x) = \int^2 \frac{s_2 + s_1 x}{C_b(x)}\,dx^2 - \int \gamma_h(x)\,dx + \frac{s_2 + s_1 \bar{x}_j}{K_j}(x - \bar{x}_j) H(x - \bar{x}_j) + c_\phi x + c_w \tag{32b}$$

with

$$\gamma_p(x) = \frac{s_1}{C_s(x)} \tag{33a}$$

$$\gamma_h(x) = -\frac{\int q(x)\,dx}{C_s(x)} \tag{33b}$$

Here, $H(x)$ is the Heaviside step function, as defined in the Appendix, and c_ϕ and c_w are integration constants that are uniquely determined by enforcing inter-element compatibility and the Dirichlet boundary conditions.

Alternatively, or when closed-form analytical solutions are not attainable, the cross-section rotations and transverse displacements can be computed numerically, pointwise, as

$$\phi(x_{i+1}) \simeq \phi(x_i) + (x_{i+1} - x_i)\chi\left(\frac{x_{i+1} + x_i}{2}\right) \tag{34a}$$

$$w(x_{i+1}) \simeq w(x_i) + (x_{i+1} - x_i)\left(\phi\left(\frac{x_{i+1} + x_i}{2}\right) - \gamma\left(\frac{x_{i+1} + x_i}{2}\right)\right) \tag{34b}$$

for $i = 1, 2, \ldots, np$, with $x_0 = 0$ and $x_{np+1} = L_e$, where $\chi = M/C_b$ and $\gamma = V/C_s$. Note that the rotation discontinuities, M_j/K_j, for $j = 1, 2, \ldots, n_c$, must be included at the crack locations. This is a simple and efficient algorithm. It is based on the midpoint Riemann sum rule of integration, although other numerical integration schemes of varying sophistication can also be adopted.

5. Numerical results and discussion

In this section, several numerical examples are analysed and discussed. For comparison purposes, the standard displacement-based finite element formulation (DBFEF), which employs C^0-continuous piecewise-linear transverse displacements and rotations, is also used in some cases. In this formulation, the cracked beams are modelled according to the classical approach, wherein the beam is partitioned into

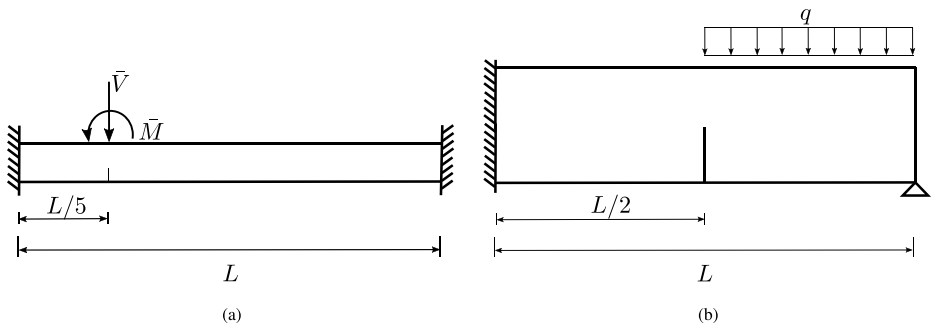

Fig. 3. Homogeneous single-cracked beams with uniform cross-section: (a) Clamped–clamped thin beam; (b) Clamped–pinned thick beam.

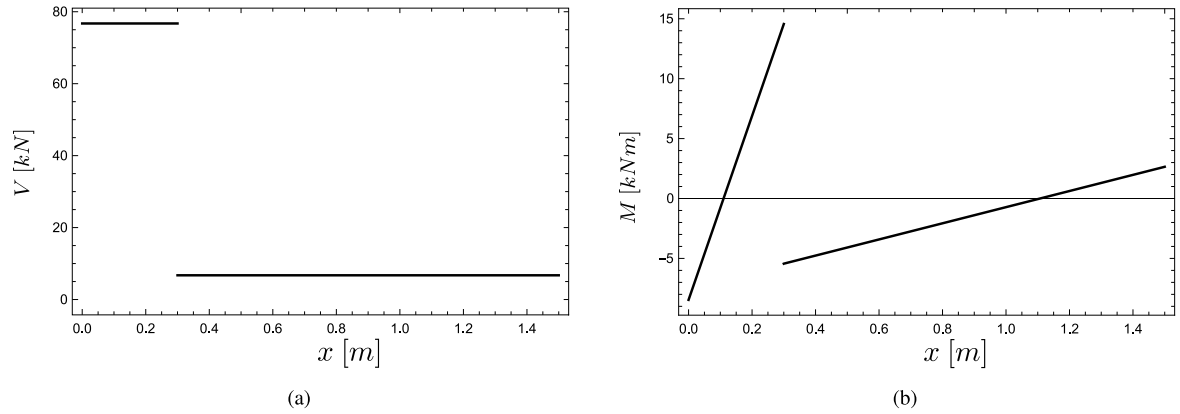

Fig. 4. Homogeneous single-cracked thin beam with uniform cross-section: (a) shear force and (b) bending moment distributions.

sub-beams at the crack locations, connected by equivalent rotational springs. It is worth noting that this formulation is known to suffer from shear-locking in the thin-beam limit (see, *e.g.*, Baier-Saip et al. (2020)).

Within the framework of the proposed formulation, unless otherwise stated, the components of matrix $\boldsymbol{F}$ and vector $\boldsymbol{d}$ were computed using a 5-point Gauss quadrature numerical integration rule.

5.1. Homogeneous single-cracked beams with uniform cross-section

Two benchmark problems previously addressed in Palmeri and Cicirello (2011) were first considered in this work, namely a clamped–clamped single-cracked thin beam and a clamped–pinned single-cracked thick beam, both having uniform rectangular cross-sections, as illustrated in Fig. 3.

In both cases, the following set of numerical data was adopted: $E = 210$ GPa, $G = 80.77$ GPa, $L = 150$ cm and $\xi = 0.5$. The local flexibilities associated with the cracks were evaluated according to Eq. (14).

For the thin-beam case, the cross-sectional dimensions were taken as $h = b = 5$ cm, and the applied shear force and bending moment were set to $\bar{V} = 70$ kN and $\bar{M} = 20$ kNm. Shear deformation effects were neglected.

For the thick-beam case, the cross-sectional dimensions were set to $h = 45$ cm and $b = 15$ cm, and the applied distributed load was set to $q = 5$ kN/cm. The shear correction factor was taken as $f_s = 5/6$.

Both cases were modelled using two equal-length elements, and the required integrations were performed exactly, both for the computation of the static fields (M and V) and the kinematic fields (ϕ and w). This procedure eliminates any numerical errors that could arise from the use of numerical integration schemes, thereby enabling a direct validation of the proposed formulation. The obtained results show a perfect agreement with the reference solutions reported in Palmeri and Cicirello (2011), and are presented in Table 1.

Table 1
Obtained results for the homogeneous single cracked beams with uniform cross-section.

Case		This study
Thin	$w(L/2)$ [mm]	2.4721
	$\phi(3L/4)$ [rad]	−0.00474
	$M(0)$ [Nm]	−8459.21
	$M^-(L/5)$ [Nm]	14561.7
	$M^+(L/5)$ [Nm]	−7459.21
	$M(L)$ [Nm]	2645.49
Thick	$w(L/2)$ [mm]	−0.0879
	$\phi(L)$ [rad]	0.00016

The shear force and bending moment distributions obtained for the thin and thick beam cases are presented in Figs. 4 and 5, respectively.

The transverse displacement and cross-section rotation fields obtained for the thin and thick beams are shown in Figs. 6 and 7, respectively. As expected, the cross-section rotations are discontinuous at the cracks.

5.2. Homogeneous multi-cracked beam with non-uniform cross-section

A tapered cantilevered homogeneous thin beam with three cracks, located at $\bar{x}_1 = 2$ m, $\bar{x}_2 = 4$ m and $\bar{x}_3 = 6$ m, and featuring a rectangular cross-section (Fig. 8) was also analysed. Two distinct loading cases were considered: (i) a concentrated shear force applied at $x = L$, and (ii) a uniformly distributed shear force applied along the entire length of the beam, as illustrated in Fig. 8. The numerical results reported in Skrinar (2013), where the beams were modelled using the Euler–Bernoulli beam theory, were taken as reference solutions. For comparison purposes, the shear deformation in both beam cases

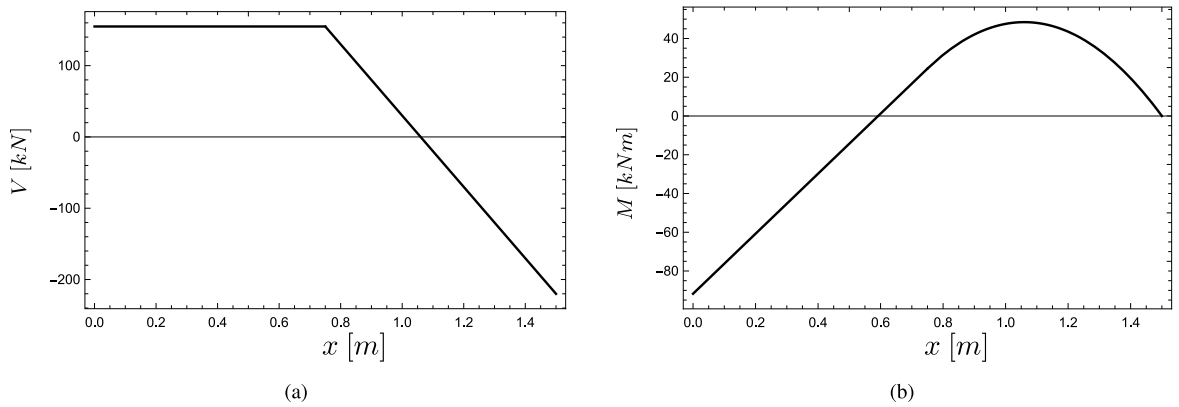

(a) (b)

Fig. 5. Homogeneous single-cracked thick beam with uniform cross-section: shear force (a) and bending moment (b) distributions.

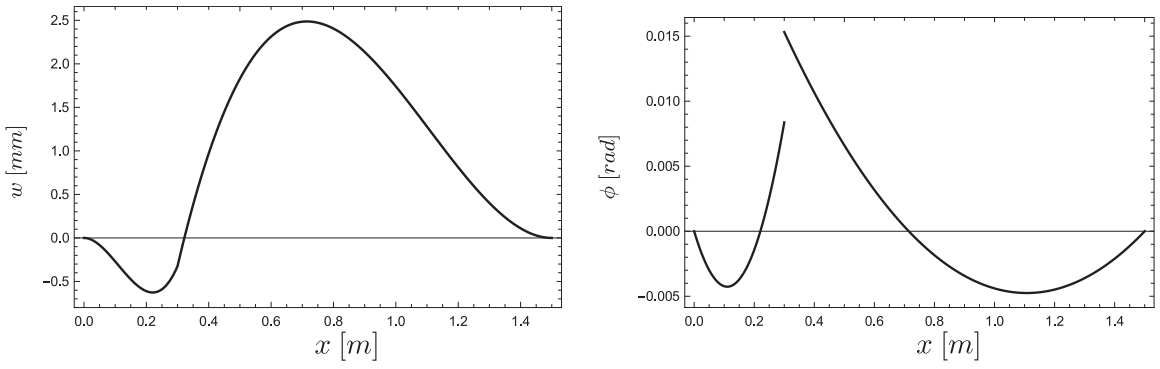

(a) (b)

Fig. 6. Homogeneous single-cracked thin beam with uniform cross-section: transverse displacements (a) and cross-section rotations (b).

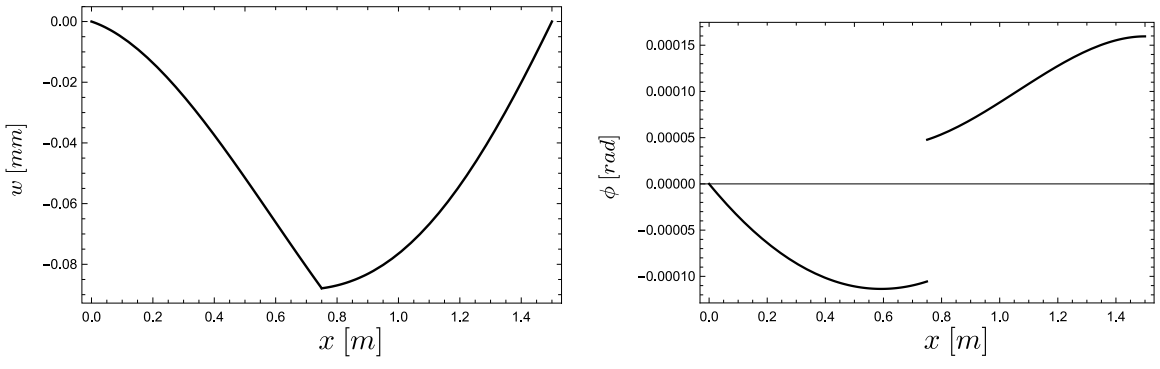

(a) (b)

Fig. 7. Homogeneous single-cracked thick beam with uniform cross-section: transverse displacements (a) and cross-section rotations (b).

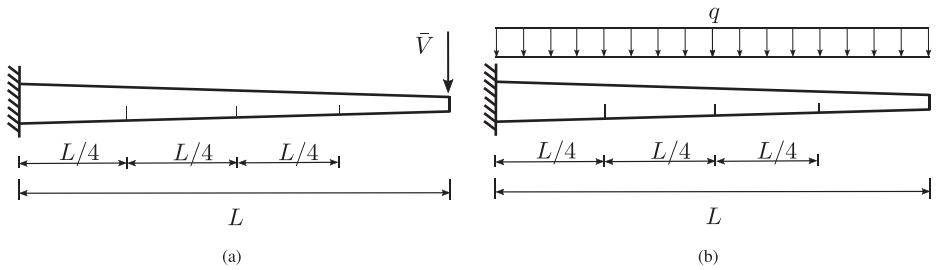

(a) (b)

Fig. 8. Homogeneous multi-cracked beam with non-uniform cross-section: (a)Tapered cantilevered thin beam with a concentrated shear force; (b) Tapered cantilevered thin beam with a uniformly distributed shear force.

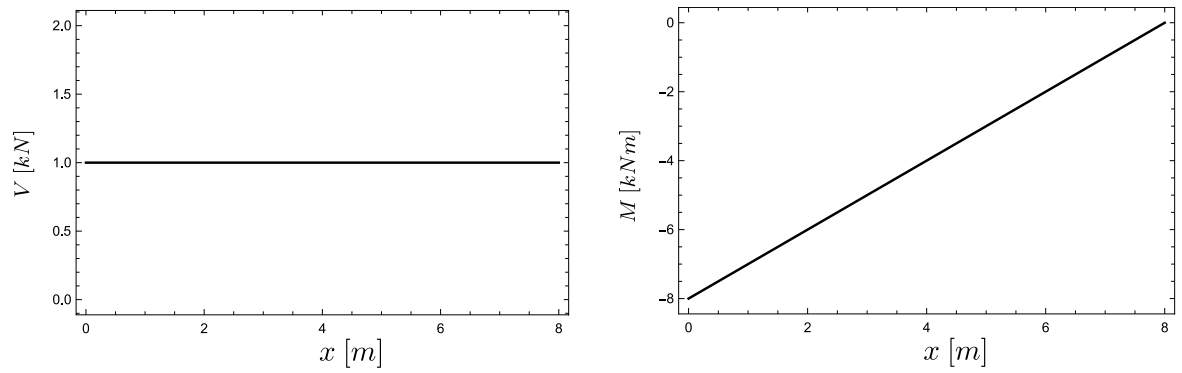

(a) (b)

Fig. 9. Cantilevered multi-cracked non-uniform beam under a concentrated shear force: shear force (a) and bending moment (b) distributions.

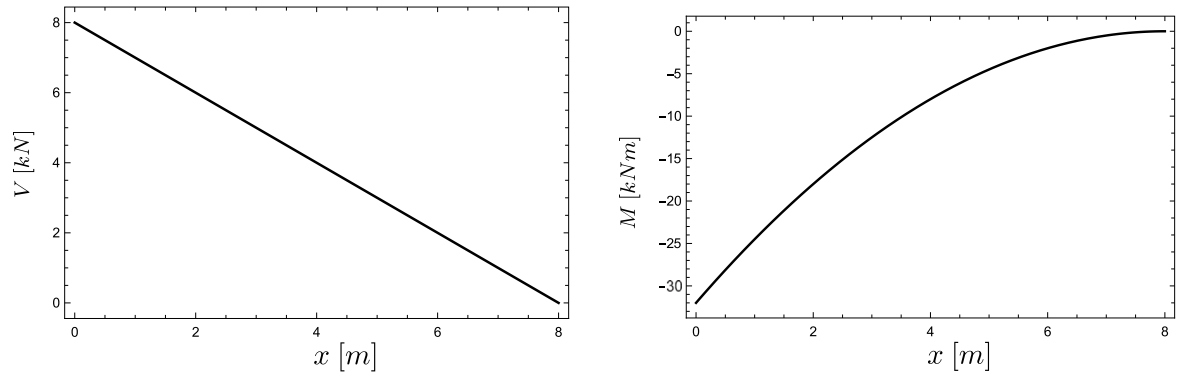

(a) (b)

Fig. 10. Cantilevered multi-cracked non-uniform beam under a distributed shear force: shear force (a) and bending moment (b) distributions.

was neglected. This was achieved by setting to zero all terms in the flexibility matrix involving the shear stiffness C_s.

In both cases, the Young's modulus and Poisson's ratio were taken as $E = 30$ GPa and $\nu = 0.1$, while the beam length was assumed to be $L = 8$ m.

The cross-section height was defined as $h(x) = h_0\,(1 - x/(2L))$, with $h_0 = h(0) = 60$ cm, and the cross-section width was set to $b = 10$ cm. The dimensionless crack depth was fixed at $\xi_j = 0.5$ for all three cracks. The concentrated load was set to $\bar{V} = 1$ kN, whereas the distributed load was taken as $q = 1$ kN/m.

The beams were discretized using single-element meshes, and the local flexibilities associated with the cracks were computed using the approaches given by Eqs. (12), (13), and (14). In the case of Okamura's formulation, based on Eq. (12), both plane stress ($\nu = 0$) and plane strain ($\nu = 0.1$) conditions were considered. It is worth noting that, although Eq. (14) is strictly valid for uniform beams, the geometry of the beams considered herein exhibits only a low degree of non-uniformity, and solely along the axial direction. As in the previous example, all required integrations were carried out exactly, both for the computation of the static fields, M and V, and for the kinematic fields, ϕ and w.

The results obtained using the proposed formulation are presented in Table 2 alongside those reported in Skrinar (2013), where the local flexibilities associated with the cracks were evaluated following Okamura's approach under plane strain conditions. As can be observed, the computed statical quantities are in perfect agreement with the reference solutions, regardless of the adopted definition of the local flexibilities — this outcome being a direct consequence of the statically determinate nature of the beam model considered. The kinematic quantities, on the other hand, although very close to each other, show a slight dependence on the chosen definition of the local flexibilities. Nevertheless, the numerical solutions obtained using Okamura's approach under plane strain conditions exhibit full agreement with the reference results reported in Skrinar (2013).

The shear force and bending moment distributions obtained for the concentrated and distributed loading cases are presented in Figs. 9 and 10, respectively. As can be observed, the static fields are C^0-continuous throughout the beam. Moreover, the shear force and bending moment distributions exhibit the expected behaviours: constant and linear variations under the concentrated load, and linear and quadratic variations under the uniformly distributed load, respectively.

The transverse displacement and cross-section rotation fields obtained for the concentrated and distributed shear force load cases, using Eq. (12) under plane strain conditions, are presented in Figs. 11 and 12, respectively. As expected, the cross-section rotations exhibit discontinuities at the crack locations.

5.3. Simply-supported uniform A-FGM beam

A simply-supported uniform square cross-section A-FGM beam subjected to a uniformly distributed load of $q = 100$ kN/m, as illustrated in Fig. 13, was also analysed. This example was taken from Molina-Villegas et al. (2024), where closed-form analytical solutions were derived, enabling validation and performance assessment of the proposed formulation when applied to A-FGM beam analysis. The edge length of the square cross-section was set to $L/20$, with $L = 1$ m.

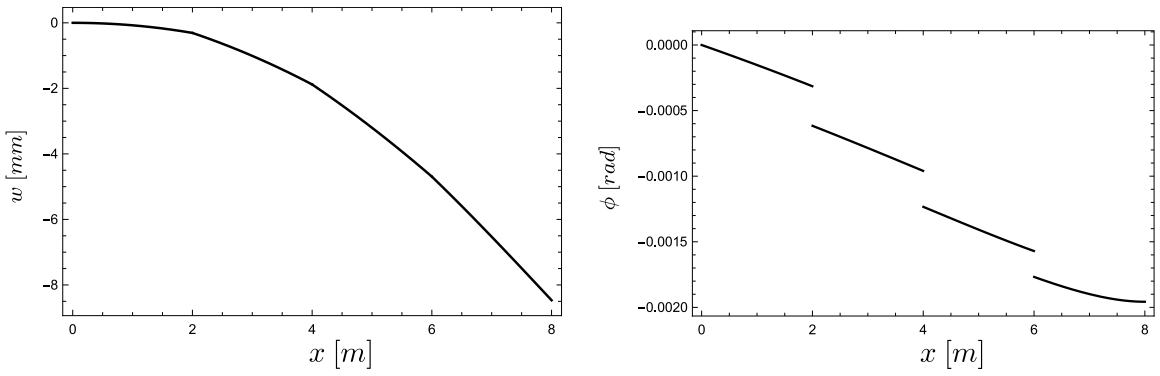

(a) (b)

Fig. 11. Cantilevered multi-cracked non-uniform beam under a concentrated shear force: transverse displacements (a) and cross-section rotations (b) based on Eq. (12) and plane strain conditions.

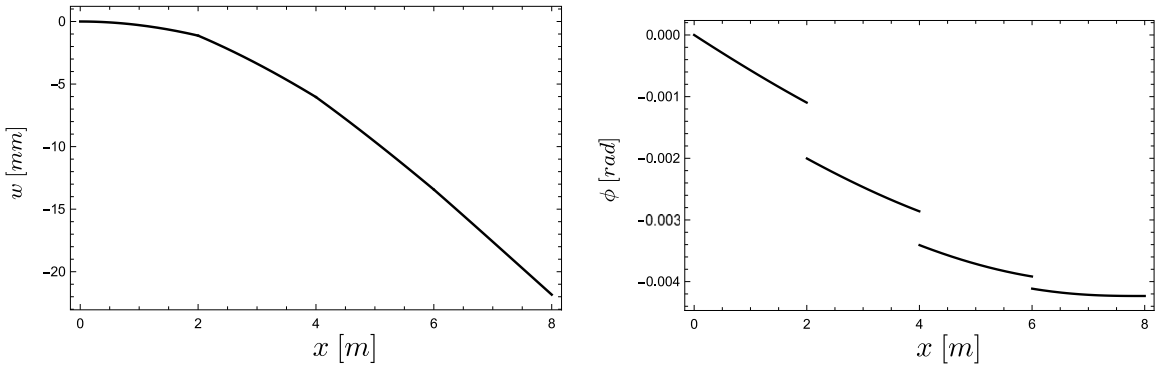

(a) (b)

Fig. 12. Cantilevered multi-cracked non-uniform beam under a distributed shear force: transverse displacements (a) and cross-section rotations (b) based on Eq. (12) and plane strain conditions.

Table 2
Obtained results for the homogeneous multi-cracked beam with non-uniform cross-section.

Case		Ref. sol. Skrinar (2013)	This study			
			Eq. (12)		Eq. (13)	Eq. (14)
			$\nu = 0.1$	$\nu = 0$		
$\bar{V} = 1$ kN	$w(\bar{x}_1)$ [mm]	−0.3085	−0.3085	−0.3085	−0.3085	−0.3085
	$w(\bar{x}_2)$ [mm]	−1.881	−1.8810	−1.8871	−1.7402	−1.8585
	$w(\bar{x}_3)$ [mm]	−4.693	−4.6927	−4.7104	−4.2832	−4.6273
	$w(L)$ [mm]	−8.466	−8.4664	−8.4997	−7.6962	−8.3433
	$\phi(L)$ [rad]	−0.001957	−0.001957	−0.001965	−0.001777	−0.001928
	$V(0)$ [N]	1000	1000	1000	1000	1000
	$M(0)$ [Nm]	−8000	−8000	−8000	−8000	−8000
$q = 1$ kN/m	$w(\bar{x}_1)$ [mm]	−1.129	−1.1291	−1.1291	−1.1292	−1.1292
	$w(\bar{x}_2)$ [mm]	−6.040	−6.0403	−6.0586	−5.6178	−5.9728
	$w(\bar{x}_3)$ [mm]	−13.432	−13.4317	−13.4793	−12.3311	−13.2559
	$w(L)$ [mm]	−21.832	−21.8323	−21.9132	−19.9616	−21.5335
	$\phi(L)$ [rad]	−0.004233	−0.004233	−0.004250	−0.003848	−0.004172
	$V(0)$ [N]	8000	8000	8000	8000	8000
	$M(0)$ [Nm]	−32000	−32000	−32000	−32000	−32000

The Poisson's ratio was taken as $\nu = 0.2$, and the Young's modulus was assumed to vary linearly along the beam's length according to $E(x) = E_0(1 - x/(2L))$, with $E_0 = 200$ GPa. A shear correction factor of $f_s = 6/7$ was adopted.

A single finite element was used for the discretization of the beam. The obtained results are reported in Table 3 alongside the analytical solutions. The transverse displacements and cross-section rotations were computed using the numerical algorithm presented above for different accuracy levels. As observed, while the shear force and bending moment solutions are exact, the accuracy of the kinematic quantities naturally depends on the number of evaluation points (np) adopted in the algorithm. Even for the coarsest level of accuracy, based on $np = 101$ discretization points, the relative errors in the transverse displacement $w(L/2)$ and rotation $\phi(0)$ are as low as 0.20% and 1.08%, respectively. It is worth noting that, in this particular case, exact analytical integration of Eq. (8) was feasible. This integration was carried out, confirming that the exact analytical kinematic solutions reported in Molina-Villegas et al. (2024) were accurately reproduced.

Table 3
Obtained results for the simply-supported uniform A-FGM beam.

	Ref. Molina-Villegas et al. (2024)	This study			
np		101	1001	10,001	40,001
$w(L/2)$ [mm]	−16.9959	−17.0298	−16.9993	−16.9962	−16.9959
$\phi(0)$ [rad]	−0.050887	−0.051435	−0.050942	−0.050893	−0.050888
$V(0)$ [kN]	50	50			
$V(L)$ [kN]	−50	−50			
$M(L/2)$ [kNm]	12.5	12.5			

Table 4
Obtained results for the clamped–clamped homogeneous multi-cracked non-uniform thick beam.

	This study		DBFEF	
n_{elem}(DOFs)	2(6)		160(320)	640(1280)
	Eq. (12)	Eq. (13)	Eq. (13)	
$w(L/2)$ [mm]	−0.1342	−0.1318	−0.1317	−0.1318
$\phi(L/2)$ [rad]	−0.000370	−0.000354	−0.000355	−0.000355
$M(0)$ [Nm]	−12847.37	−13010.30	−13016.22	−13012.78
$M(L/2)$ [Nm]	4778.47	4746.79	4669.12	4727.28
$M(L)$ [Nm]	−2595.70	−2496.10	−2403.38	−2473.03
$V(0)$ [N]	70 503.33	71 028.38	73 412.12	71 626.37
$V(L)$ [N]	−29496.67	−28971.62	−35233.09	−30579.05

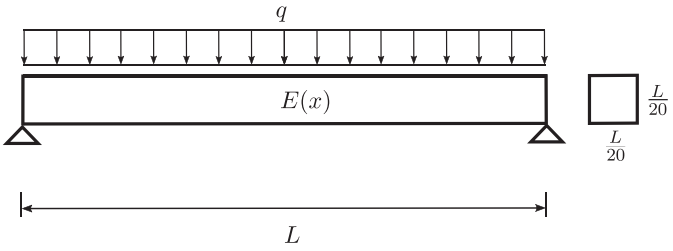

Fig. 13. Simply-supported uniform A-FGM beam.

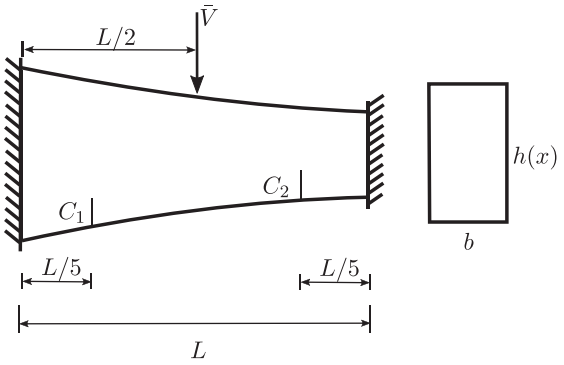

Fig. 14. Clamped–clamped homogeneous multi-cracked non-uniform thick beam.

5.4. Clamped–clamped homogeneous multi-cracked non-uniform beam

A clamped–clamped non-uniform thick beam with two cracks, C_1 and C_2, located at $\bar{x}_1 = L/5$ and $\bar{x}_2 = 4L/5$, and subjected to a transverse tip load, as illustrated in Fig. 14, was also analysed. The following set of numerical data was adopted: $L = 50$ cm, $\bar{V} = 100$ kN, $E = 70$ GPa and $\nu = 0.17$. The cross-section height was assumed to vary quadratically according to $h(x) = h_0\,(1 - x/(2L))^2$, with $h_0 = h(0) = 20$ cm, while the cross-section width was set to $b = 10$ cm. A shear correction factor of $f_s = 5/6$ was considered. The dimensionless crack depths were taken as $\xi_1 = 0.2$ and $\xi_2 = 0.6$.

Since no reference solution is available for this problem, the beam was analysed using both the proposed formulation and the DBFEF. Within the framework of the proposed formulation, the beam was discretized into two equal-length elements, and the transverse displacements and cross-section rotations were computed using the previously presented algorithm with $np = 1001$ points. For the DBFEF, two distinct uniform meshes were employed: one with 160 elements (320 DOFs), and a finer mesh with 640 elements (1280 DOFs), with all required integrations being performed exactly. Owing to the non-uniformity of the beam, in the proposed formulation the local flexibilities associated with the cracks were evaluated using Eq. (12) under plane strain conditions and Eq. (13), whereas in the DBFEF the local stiffnesses were computed exclusively according to Eq. (13).

Several kinematic and static quantities were computed as presented in Table 4. First, the results produced by the proposed formulation are in excellent agreement with those obtained using the DBFEF. Secondly, all results – both static and kinematic – computed even with the 160-element mesh (320 DOFs) are less accurate than those provided by the proposed formulation using a very coarse 2-element mesh (only 6 DOFs). The DBFEF distributions of shear force and bending moment, in particular, are noticeably less accurate than the corresponding results obtained with the proposed formulation, even when a very fine mesh is employed. This discrepancy arises because, in the DBFEF, the equilibrium equations are satisfied only in the weak sense. Consequently, the bending moment fields are piecewise constant and inherently discontinuous between adjacent elements. The bending moment values at midspan, $M(L/2)$, reported for the DBFEF were computed by averaging the bending moments of the two neighbouring elements at $x = L/2$.

The shear force and bending moment distributions obtained using the proposed formulation with Eq. (13) are shown in Fig. 15. As can be observed, both fields are C^0-continuous, except for the shear force at $x = L/2$, where a discontinuity occurs due to the applied transverse load.

The transverse displacements and cross-section rotations obtained using the proposed formulation with Eq. (13) are shown in Fig. 16. As expected, the rotations exhibit discontinuities at the crack locations. Moreover, although the cross-section rotation vanishes at $x = 0$ and $x = L$ (the beam supports), the derivative of the transverse displacement, u', does not. This behaviour arises from the nonzero shear deformations at the beam supports (see Fig. 17). Finally, as expected, the shear deformation is discontinuous at $x = L/2$, reflecting the discontinuous nature of the shear force field induced by the concentrated shear load applied at that location.

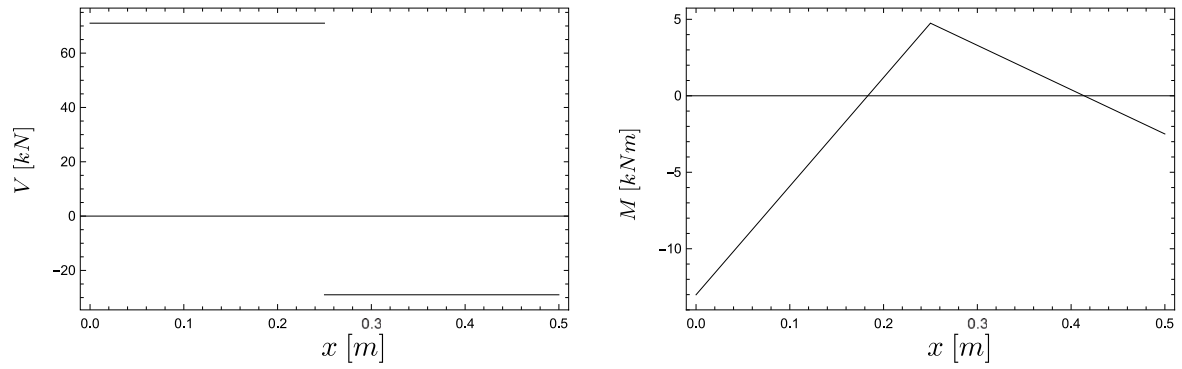

(a) (b)

Fig. 15. Clamped–clamped multi-cracked non-uniform thick beam: shear force (a) and bending moment (b) distributions obtained using the proposed formulation with Eq. (13).

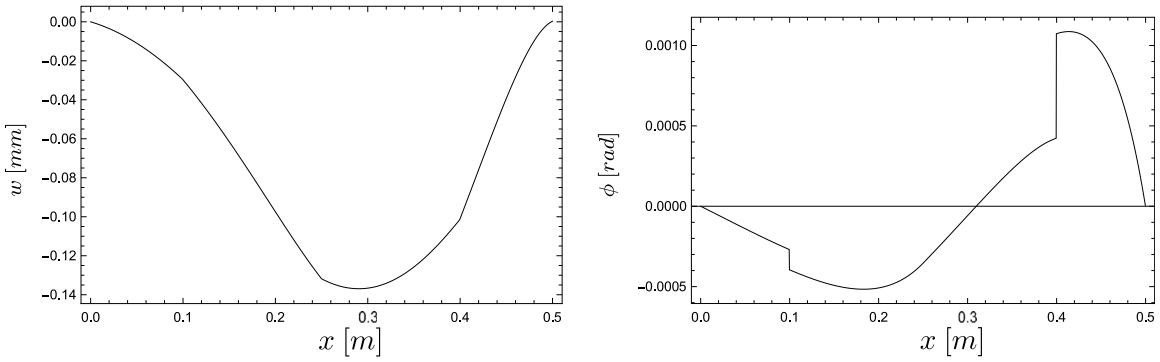

(a) (b)

Fig. 16. Clamped–clamped multi-cracked non-uniform thick beam: transverse displacements (a) and cross-section rotations (b) obtained using the proposed formulation with Eq. (13).

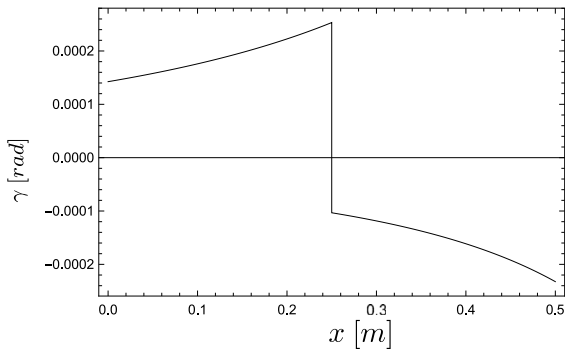

Fig. 17. Clamped–clamped multi-cracked non-uniform thick beam: shear deformation fields obtained using the proposed formulation with Eq. (13).

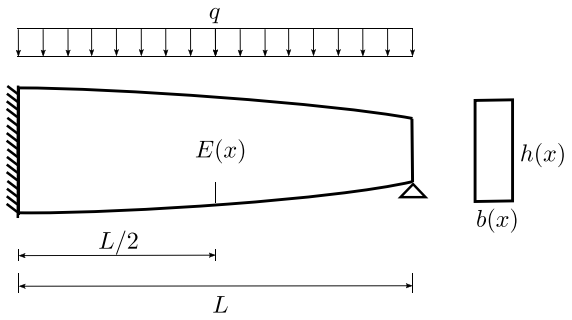

Fig. 18. Clamped–pinned A-FGM single-cracked non-uniform beam.

5.5. Clamped–pinned A-FGM single-cracked non-uniform beam

Finally, a clamped–pinned A-FGM non-uniform beam with a single crack subjected to a uniformly distributed transverse load, as depicted in Fig. 18, was analysed. The crack was located at $\bar{x}_1 = L/2$, with a dimensionless crack depth of $\xi = 0.5$. The beam length was taken as $L = 2$ m and the applied distributed load was set to $q = 100$ kN/m.

The Young's modulus was assumed to vary quadratically along the beam's length as $E(x) = E_0 + (E_1 - E_0)(x/L)^2$, with $E_0 = 200$ GPa and $E_1 = 70$ GPa, while the Poisson's ratio was taken as $\nu = 1/3$. The cross-section height was assumed to vary quadratically, $h(x) = h_0\left(1 - 2/3(x/L)^2\right)$, with $h_0 = L/10$, whereas the cross-section width was assumed to vary linearly along the length as $b(x) = b_0\,(1 - 1/2(x/L))$, with $b_0 = L/20$. The adopted shear correction factor was $f_s = 5/6$.

Since no reference solution is available for this problem, the beam was modelled, as in the previous example, using both the proposed

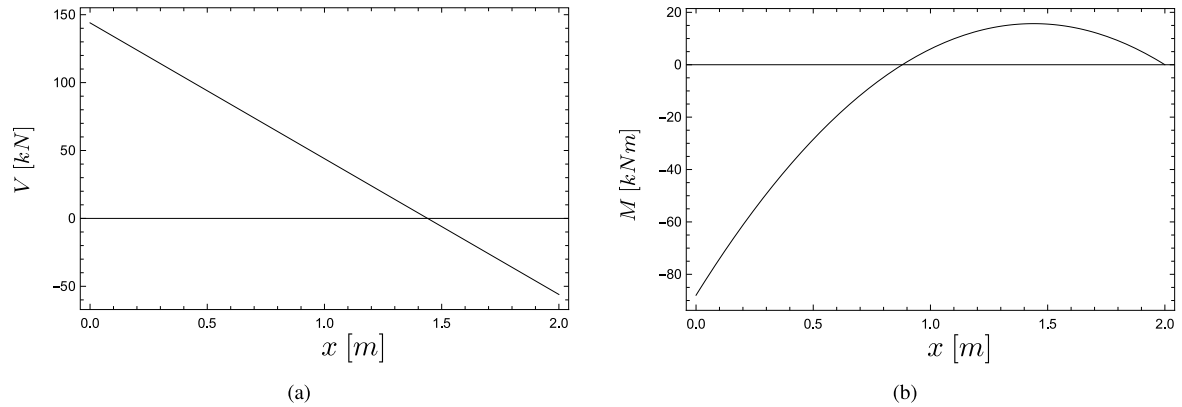

(a) (b)

Fig. 19. Clamped–pinned A-FGM single-cracked non-uniform beam: shear force (a) and bending moment (b) distributions obtained using the proposed formulation with Eq. (13) and the 10-point Gauss quadrature.

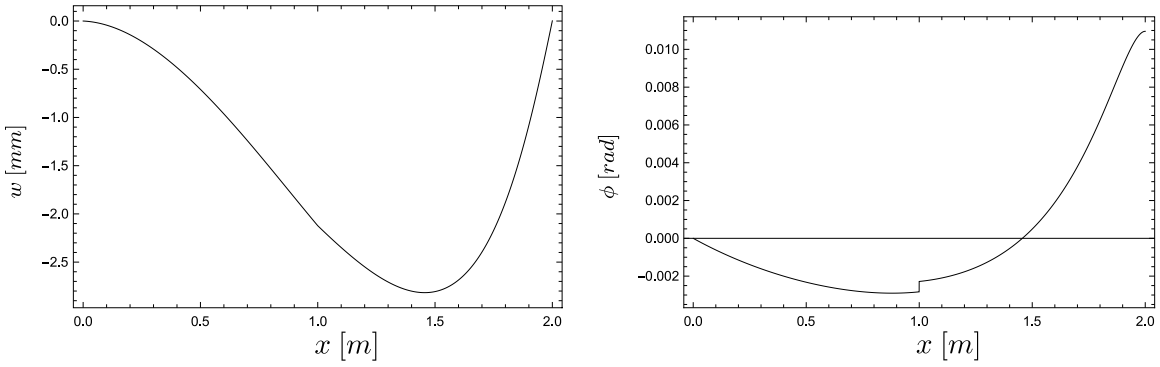

(a) (b)

Fig. 20. Clamped–pinned A-FGM single-cracked non-uniform beam: transverse displacements (a) and cross-section rotations (b) obtained using the proposed formulation with Eq. (13), a 10-point Gauss quadrature and $np = 10001$.

Table 5
Obtained results for the clamped–pinned A-FGM single-cracked non-uniform beam.

	This study		DBFEF	
n_{elem}(DOFs)	1(3)		128(256)	1024(2048)
Quadrature	5-point Gauss	10-point Gauss	Exact	
$w(L/2)$ [mm]	−2.1123	−2.1224	−2.1157	−2.1223
$\phi(L)$ [rad]	0.011038	0.010955	0.010872	0.010953
$M(0)$ [Nm]	−87728.61	−87989.86	−86804.88	−87867.52
$M(L/2)$ [Nm]	6135.69	6005.07	6026.91	6005.19
$M(L)$ [Nm]	0	0	393.43	54.06
$V(0)$ [N]	143864.31	143994.93	206995.86	151975.97
$V(L)$ [N]	−56135.69	−56005.07	49508.32	44646.19

formulation and the standard DBFEF. Within the framework of the proposed formulation, the beam was discretized using a single-element mesh (3 DOFs). Two numerical integration schemes were considered for comparison, namely, 5-point and 10-point Gauss quadratures. The transverse displacements and cross-section rotations were computed using the previously described algorithm with $np = 10001$ points. As for the DBFEF, uniform meshes with 128 (256 DOFs) and 1024 (2048 DOFs) elements were adopted, with the required integrations being carried out exactly. The local flexibilities and stiffnesses associated with the cracks were evaluated according to Eq. (13).

The obtained results are presented in Table 5, where several kinematic and static quantities are compared. As can be observed, the results obtained with the proposed formulation are in excellent agreement with those produced by the DBFEF. Moreover, even the results (for both static and kinematic quantities) obtained using the 128-element mesh (256 DOFs) are less accurate than those provided by the proposed formulation on a single-element mesh (3 DOFs) with a 10-point Gauss quadrature. Regarding the shear force and bending moment distributions computed with the DBFEF, not even the highly refined mesh of 1024 elements was sufficient to achieve the same level of accuracy as that of the proposed formulation. It is also worth noting that, even for the most refined DBFEF mesh, the bending moment at the free end, $M(L)$, does not satisfy the equilibrium boundary condition $M(L) = 0$.

The shear force and bending moment solutions obtained using the proposed formulation with Eq. (13) and the 10-point Gauss quadrature are shown in Fig. 19. As can be observed, the resulting fields are C^0-continuous, in clear contrast to those produced by the standard DBFEF.

The transverse displacements and cross-section rotations computed using the proposed formulation with Eq. (13), in conjunction with the 10-point Gauss quadrature and $np = 10001$, are shown in Fig. 20.

As expected, the cross-section rotation is discontinuous at the crack. All kinematic boundary conditions, namely $w(0) = 0$, $w(L) = 0$ and $\phi(0) = 0$, are satisfied.

6. Conclusions

A new finite element formulation for the static analysis of multi-cracked, non-uniform, functionally graded Timoshenko beams has been presented. The cracks, assumed to remain open throughout the loading process, were modelled using a discrete spring approach, in which Dirac delta generalized functions were incorporated into the beam's bending flexibility. The equivalent flexibilities associated with the cracks were evaluated according to various formulations available in the literature for rectangular cross-section beams. The proposed formulation, derived from a complementary energy-based variational principle, ensures statically admissible solutions — that is, solutions satisfying all equilibrium equations in their strong form. The formulation was applied to the analysis of beams exhibiting diverse cross-section variations, crack configurations, and material gradations (either homogeneous or axially functionally graded). Comparisons with reference solutions and with results from the standard displacement-based finite element formulation confirmed the accuracy and efficiency of the proposed approach, which was shown to yield highly accurate results for both thin and thick beams, even when employing very coarse meshes.

CRediT authorship contribution statement

H.A.F.A. Santos: Writing – review & editing, Writing – original draft, Visualization, Validation, Methodology, Investigation, Formal analysis, Conceptualization. **V.V. Silberschmidt:** Writing – review & editing, Validation, Methodology, Conceptualization.

Declaration of competing interest

The authors declare that they have no known competing financial interests or personal relationships that could have appeared to influence the work reported in this paper.

Appendix. Generalized dirac delta and heaviside step functions

The generalized Dirac delta function is defined according to

$$\delta(x-a) := \begin{cases} 0 & \text{for } x \neq a \\ \infty & \text{for } x = a \end{cases}$$

and satisfies the following properties

$$\int_{a-\varepsilon}^{a+\varepsilon} \delta(x-a)\, dx = 1,\ \varepsilon > 0$$

and

$$\int_{a-\varepsilon}^{a+\varepsilon} f(x)\delta(x-a)\, dx = f(a),\ \varepsilon > 0$$

The Heaviside step function is defined according to

$$H(x-a) := \begin{cases} 0 & \text{for } x < a \\ 1 & \text{for } x \geq a \end{cases}$$

It can be shown that

$$H(x-a) = \int_{a-\varepsilon}^{x} \delta(x-a)\, dx,\ \varepsilon > 0$$

or

$$\frac{dH(x-a)}{dx} = \delta(x-a)$$

Data availability

Data will be made available on request.

References

Alshorbagy, A.E., Eltaher, M.A., Mahmoud, F., 2011. Free vibration characteristics of a functionally graded beam by finite element method. Appl. Math. Model. 35 (1), 412–425.

Baier-Saip, J.A., Baier, P.A., Faria, A.R., Oliveira, J.C., Baier, H., 2020. Shear locking in one-dimensional finite element methods. Eur. J. Mech. A Solids 79, 103871.

Bilello, C., 2001. Theoretical and Experimental Investigation on Damaged Beams Under Moving Systems (Ph.D. thesis). University of Palermo.

Biondi, B., Caddemi, S., 2005. Closed form solutions of Euler-Bernoulli beams with singularities. Int. J. Solids Struct. 42 (9–10), 3027–3044.

Biondi, B., Caddemi, S., 2007. Euler-Bernoulli beams with multiple singularities in the flexural stiffness. Eur. J. Mech. A Solids 26 (5), 789–809.

Caddemi, S., Calio, I., 2009. Exact closed-form solution for the vibration modes of the Euler-Bernoulli beam with multiple open cracks. J. Sound Vib. 327 (3–5), 473–489.

Caddemi, S., Morassi, A., 2013. Multi-cracked Euler-Bernoulli beams: Mathematical modelling and exact solutions. Int. J. Solids Struct. 50 (6), 944–956.

Chondros, T.G., Dimarogonas, A.D., Yao, J., 1998. A continuous cracked beam vibration theory. J. Sound Vib. 215 (1), 17–34.

Christides, S., Barr, A.D.S., 1984. One-dimensional theory of cracked Bernoulli-Euler beams. Int. J. Mech. Sci. 26 (11), 639–648.

Cicirello, A., Palmeri, A., 2014. Static analysis of Euler-Bernoulli beams with multiple unilateral cracks under combined axial and transverse loads. Int. J. Solids Struct. 51 (5), 1020–1029.

Dimarogonas, A.D., 1996. Vibration of cracked structures: a state of the art review. Eng. Fract. Mech. 55 (5), 831–857.

Dimarogonas, A.D., Paipetis, S.S., Chondros, T.G., 2013. Analytical Methods in Rotor Dynamics. Springer Science & Business Media.

Donà, M., Palmeri, A., Lombardo, M., Cicirello, A., 2015. An efficient two-node finite element formulation of multi-damaged beams including shear deformation and rotatory inertia. Comput. Struct. 147, 96–106.

Eftekhari, S., 2015. A differential quadrature procedure with regularization of the Dirac-delta function for numerical solution of moving load problem. Lat. Am. J. Solids Struct. 12 (7), 1241–1265.

Failla, G., Impollonia, N., 2012. General finite element description for non-uniform and discontinuous beam elements. Arch. Appl. Mech. 82, 43–67.

Friswell, M.I., Penny, J.E.T., 2002. Crack modeling for structural health monitoring. Struct. Health Monit. 1 (2), 139–148.

Hassaine, N., Dahak, M., Touat, N., Khatir, S., Benaissa, B., Cuong-Le, T., 2025. Damage identification in functionally graded material beam structures based on frequency analysis and AOA-ANN. Mech. Based Des. Struct. Mach. 1–21.

Hughes, T.J.R., 2012. The Finite Element Method: Linear Static and Dynamic Finite Element Analysis. Courier Corporation.

Kitipornchai, S., Ke, L.-L., Yang, J., Xiang, Y., 2009. Nonlinear vibration of edge cracked functionally graded Timoshenko beams. J. Sound Vib. 324 (3–5), 962–982.

Lien, T.V., Duc, N.T., Khiem, N.T., 2017. Free vibration analysis of multiple cracked functionally graded Timoshenko beams. Lat. Am. J. Solids Struct. 14, 1752–1766.

Molina-Villegas, J.C., Ortega, J.E.B., Soto, S.B., 2024. Closed-form solutions for axially non-uniform Timoshenko beams and frames under static loading. Compos. Struct. 337, 118078.

Nguyen, K.V., Dao, T.T.B., Nguyen, Q.V., 2024. Exact solution for mode shapes of cracked nonuniform axially functionally graded beams. Mech. Res. Commun. 139, 104306.

Okamura, H., Liu, H.W., Chu, C.S., Liebowitz, H., 1969. A cracked column under compression. Eng. Fract. Mech. 1 (3), 547–564.

Ostachowicz, W.M., Krawczuk, M., 1991. Analysis of the effect of cracks on the natural frequencies of a cantilever beam. J. Sound Vib. 150 (2), 191–201.

Palmeri, A., Cicirello, A., 2011. Physically-based Dirac's delta functions in the static analysis of multi-cracked Euler-Bernoulli and Timoshenko beams. Int. J. Solids Struct. 48, 2184–2195.

Pandey, A.K., Biswas, M., 1994. Damage detection in structures using changes in flexibility. J. Sound Vib. 169 (1), 3–17.

Papadopoulos, C.A., 2004. Some comments on the calculation of the local flexibility of cracked shafts. J. Sound Vib. 278 (4–5), 1205–1211.

Petroski, H.J., 1981. Simple static and dynamic models for the cracked elastic beam. Int. J. Fract. 17 (4), R71–R76.

Rajasekaran, S., Khaniki, H.B., 2018. Free vibration analysis of bi-directional functionally graded single/multi-cracked beams. Int. J. Mech. Sci. 144, 341–356.

Rizos, P.F., Aspragathos, N., Dimarogonas, A.D., 1990. Identification of crack location and magnitude in a cantilever beam from the vibration modes. J. Sound Vib. 138 (3), 381–388.

Santos, H.A.F.A., 2011. Complementary-energy methods for geometrically non-linear structural models: an overview and recent developments in the analysis of frames. Arch. Comput. Methods Eng. 18 (4), 405–440.

Santos, H.A.F.A., 2012. Variationally consistent force-based finite element method for the geometrically non-linear analysis of Euler-Bernoulli framed structures. Finite Elem. Anal. Des. 53, 24–36.
Santos, H.A.F.A., 2015. A novel updated Lagrangian complementary energy-based formulation for the elastica problem: force-based finite element model. Acta Mech. 226 (4), 1133–1151.
Santos, H.A.F.A., 2020. Buckling analysis of layered composite beams with interlayer slip: A force-based finite element formulation. Structures 25, 542–553.
Santos, H.A.F.A., 2024. A new finite element formulation for the dynamic analysis of beams under moving loads. Comput. Struct. 298, 107347.
Santos, H.A.F.A., Pimenta, P.M., Almeida, J.P.M., 2011. A hybrid-mixed finite element formulation for the geometrically exact analysis of three-dimensional framed structures. Comput. Mech. 48, 591–613.
Santos, H.A.F.A., Silberschmidt, V.V., 2014. Hybrid equilibrium finite element formulation for composite beams with partial interaction. Compos. Struct. 108, 646–656.
Santos, H.A.F.A., Silberschmidt, V.V., 2024. Assessment of multi-cracked non-uniform FGM beams using an equilibrium-based finite element formulation. Procedia Struct. Integr. 66, 195–204.
Shabani, S., Cunedioglu, Y., 2020a. Free vibration analysis of cracked functionally graded non-uniform beams. Mater. Res. Express 7 (1), 015707.
Shabani, S., Cunedioglu, Y., 2020b. Free vibration analysis of functionally graded beams with cracks. J. Appl. Comput. Mech. 6 (4), 908–919.
Sinha, G.P., Kumar, B., 2021. Review on vibration analysis of functionally graded material structural components with cracks. J. Vib. Eng. Technol. 9, 23–49.
Skrinar, M., 2013. Computational analysis of multi-stepped beams and beams with linearly-varying heights implementing closed-form finite element formulation for multi-cracked beam elements. Int. J. Solids Struct. 50 (14–15), 2527–2541.
Skrinar, M., 2019. On the application of the simplified crack model in the bending, free vibration and buckling analysis of beams with linear variation of widths. Period. Polytech. Civ. Eng. 63 (2), 423–431.
Skrinar, M., Imamovic, D., 2018. On the bending analysis of multi-cracked slender beams with continuous height variations. Period. Polytech. Civ. Eng. 62 (4), 873–880.
Washizu, K., 1975. Variational Methods in Elasticity and Plasticity. Pergamon Press.
Wei, D., Liu, Y., Xiang, Z., 2012. An analytical method for free vibration analysis of functionally graded beams with edge cracks. J. Sound Vib. 331 (7), 1686–1700.
Yang, J., Chen, Y., 2008. Free vibration and buckling analyses of functionally graded beams with edge cracks. Compos. Struct. 83 (1), 48–60.
Yang, X., Huang, J., Ouyang, Y., 2016. Bending of Timoshenko beam with effect of crack gap based on equivalent spring model. Appl. Math. Mech. 37, 513–528.
Zhu, L.-F., Ke, L.-L., Zhu, X.-Q., Xiang, Y., Wang, Y.-S., 2019. Crack identification of functionally graded beams using continuous wavelet transform. Compos. Struct. 210, 473–485.
Zienkiewicz, O.C., Taylor, R.L., 2005. The Finite Element Method for Solid and Structural Mechanics. Elsevier.
Zienkiewicz, O.C., Taylor, R.L., Zhu, J.Z., 2005. The Finite Element Method: Its Basis and Fundamentals. Elsevier.